GEOLOGICA CARPATHICA, 49, 5, BRATISLAVA, OCTOBER 1998
315–327

POST-OROGENIC UPLIFT-INDUCED EXTENSION: A KINEMATIC MODEL FOR THE PLIOCENE TO RECENT TECTONIC EVOLUTION OF THE EASTERN CARPATHIANS (ROMANIA)

RADU GÎRBACEA*, WOLFGANG FRISCH and HANS-GERT LINZER**

Institut für Geologie, Universität Tübingen, Sigwartstr. 10, D-72076 Tübingen, Germany

(Manuscript received January 12, 1998; accepted in revised form September 1, 1998)

Abstract: We propose a new tectonic model for the Pliocene to Recent tectonic evolution of the Eastern Carpathians, especially for the formation of the Braşov-Gheorghieni basin system in the hinterland and for the shortening in the foreland during the "Valachian Phase" of deformation. Kinematic analysis of fault-slip data indicates the formation of the Braşov-Gheorghieni basins due to NW-SE oriented extension, but with joints displaying varying orientations suggesting regional uplift as the source of extension. The trend of regional folds in the foreland indicates NW-SE oriented shortening. The sedimentation rate of coarse material in the foreland basin reflects a high post-Miocene rate of uplift, very accelerated during Pliocene–Quaternary time. The seismological data show active offset along two strike-slip faults (the Trotuş and Intramoesian faults), which border both the region of extension in the hinterland and the area of shortening in the foreland. A third strike-slip fault (the Sinaia Fault) is constrained south of the Braşov-Gheorghieni basins by kinematic and seismological data. All these observations have been combined in the following new tectonic model: succeeding the continental collision in Miocene, a very high rate of uplift occurred in the Eastern Carpathians during Pliocene–Quaternary time. The uplift induced gravitational mass transfer from the uplifted area, which had a high potential energy, towards the surrounding areas with low potential energy. The mass transfer took place through the southeastward motion of a crustal block between the Trotuş sinistral and the Sinaia dextral strike-slip faults above an older, reactivated detachment horizon of the Eastern Carpathians fold-and-thrust belt. The motion of this crustal block resulted in extension in the hinterland and the formation of the Braşov-Gheorghieni basin system; the extension was accommodated by shortening in the foreland.

Key words: Pliocene, Recent, Eastern Carpathians, Braşov-Gheorghieni basins, post-orogenic uplift, extension, shortening.

Introduction

This paper regards the last stage of tectonic evolution of the Eastern Carpathians from Pliocene to Recent, addressing mainly the problem of the formation of the Braşov-Gheorghieni basin system (Fig. 1a). This system consists of a series of intramontaneous basins with up to 1000 m subsidence (Bandrabur & Codarcea 1974), superimposed on older Cretaceous-Tertiary structures. The basins were formed in the Eastern Carpathians hinterland in a "post-orogenic" stage, after the oceanic crust was consumed and continental collision occurred in Miocene time (Csontos 1995). Another important characteristic feature of this last stage of tectonic evolution is the folding of Plio-Pleistocene formations in the Eastern Carpathians foreland during the "Valachian Phase" of deformation, described and characterized by Dumitrescu & Săndulescu (1968) and Săndulescu (1984). Also, in Pliocene–Quaternary time up to 10 km of sediment accumulation is recorded in the Eastern Carpathians foreland (Paraschiv 1979), while in the hinterland alkaline basaltic and calc-alkaline andesitic volcanism occurred in the Perşani and Harghita Mts. (Peltz et al. 1971; Pécskay et al. 1995). The Vrancea Zone must also be mentioned here as the place of strong seismicity with both crustal and intermediate-depth earthquakes. The active tectonics is reflected mainly by vertical movements and seismic activity.

All the mentioned Pliocene-Quaternary features are located in the southern Eastern Carpathians, between the Trotuş and the Intramoesian strike-slip faults (Fig. 1a). The aim of this paper is to interpret the formation of the hinterland Braşov-Gheorghieni basin system in terms of its kinematics and relation with the folded foreland. Our study is mainly based on kinematic analysis of fault-slip and joint data, as well as on reinterpretation of published profiles and seismological data. The fault-slip and joint data were collected from Pliocene-Quaternary sedimentary and volcanic rocks from the Braşov-Gheorghieni basins and Perşani Mountains, but also from older rocks. In this latter case we used only the youngest data sets which were separated on overprinting criteria observed in outcrops.

Tectonic setting

The Eastern Carpathians are part of the Carpathian chain, which extends over more than 1700 km between the Eastern

*Present address: Rock Fracture Project, Geological and Environmental Sciences, Stanford University, Stanford, California 94305-2115; radu@pangea.stanford.edu
**Present address: Rohöl - Aufsuchungs A.G., Schwarzenbergplatz 16, A-1015 Wien, Austria

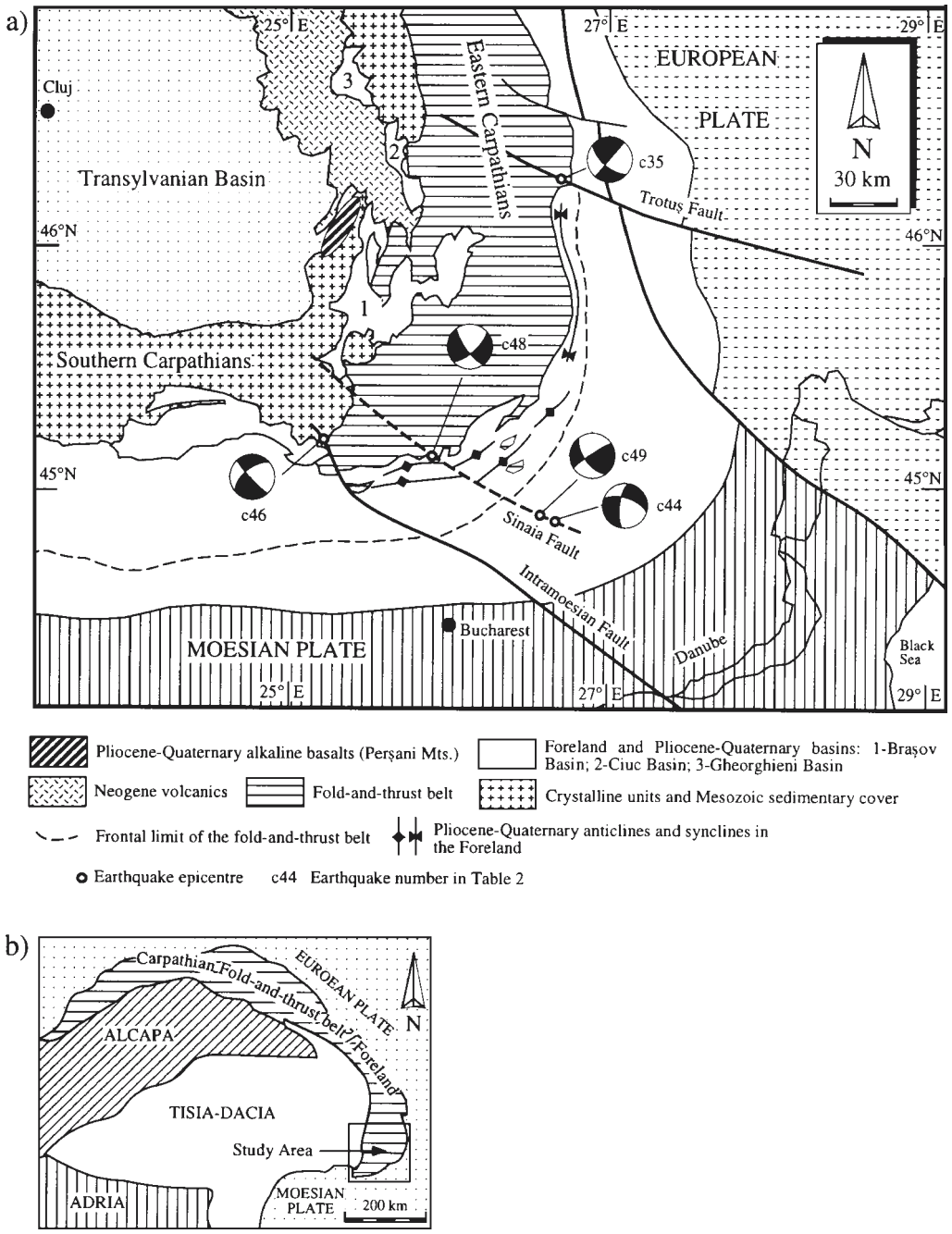

Fig. 1. a) Location of the study area in the southern Eastern Carpathians and tectonic map showing the Pliocene-Quaternary features between the Trotuş and the Intramoesian strike-slip faults (after Bandrabur et al. 1971; Săndulescu et al. 1978; Săndulescu 1984). The position of the dextral Sinaia Fault is inferred from fault-slip data from the southern Braşov Basin (site 107-95 in Fig. 2) and seismological data (see Table 2). **b)** Tectonic blocks (Alcapa and Tisia-Dacia) whose convergence and continental collision with the European and Moesian plates resulted in the formation of the Carpathian arc during Tertiary times (after Csontos 1995).

Alps and the Balkans. The present tectonic setting of the Carpathians is the result of convergence and continental collision of two continental fragments (the Tisia-Dacia and Alcapa microcontinents, Fig. 1b) with the European Plate, following retreating subduction (Royden 1993) and closure of a basin floored by oceanic or thinned continental crust (Csontos 1995; Linzer 1996). The first stage of continental collision between the Tisia-Dacia and the European plates is indicated in the Eastern Carpathians by the change from flysch-type to molasse-type sedimentation in Early Miocene (Burdigalian) time (Csontos et al. 1992).

The Trotuş Fault (Fig. 1a) is an important structure in the Eastern Carpathians, since the orogen displays different characteristics north and south of it. In the northern Eastern Carpathians the crust attains up to 56 km thickness (Starostenko & Kharitonov 1996). The isostatic response exhumed large metamorphic complexes (the Median Dacides after Săndulescu 1984), with the present surface reaching up to 2500 m alti-

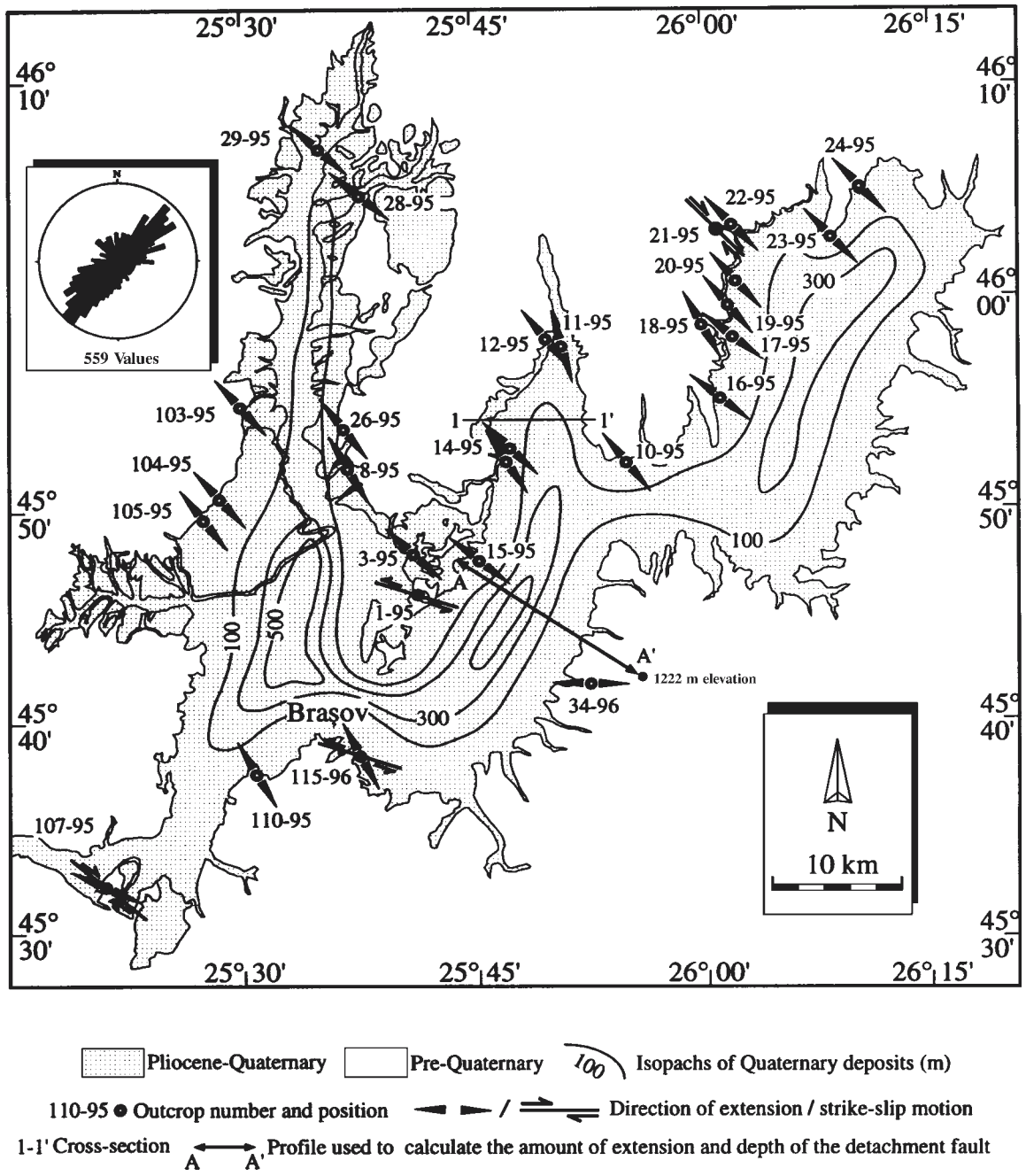

Fig. 2. Directions of extension recorded in Pliocene-Quaternary rocks or separated as the youngest recorded deformation in pre-Pliocene rocks from the Braşov Basin. The kinematic analysis is based on fault-slip and joint data (see Table 1 and Fig. 13 for results and graphical presentation of data sets). The rose diagram shows the orientation of all measured joint planes, indicating that most of them formed due to NW-SE oriented extension.

tude. Apatite cooling ages indicate an exhumation pulse around 10 Ma (Sanders & Andriessen 1996). Post-collisional shortening at the frontal wedge of the northern Eastern Carpathians occurred until 11 Ma (i.e. Sarmatian) after Roure et al. (1993), inferred from the age of the youngest sediments deposited on the European Plate which were overthrust by the orogenic front. The foreland basin contains only Sarmatian formations, in which no deformation has been recorded (Săndulescu et al. 1981).

South of the Trotuş Fault the Pliocene-Quaternary features which are the subject of this work, are exposed: the Braşov-Gheorghieni basin system and the folded foreland formations (Fig. 1a). The foreland displays a high rate of subsidence, with up to 10,000 m of molasse-type sedimentary rocks deposited during Sarmatian–Quaternary time (Săndulescu et al. 1995). In the Vrancea Zone focal mechanism solutions of intermediate-depth earthquakes indicate a vertical dense slab in the lithosphere (Fuchs et al. 1979; Oncescu 1984). The crustal thickness in the southern Eastern Carpathians does not exceed 45 km (Rădulescu et al. 1976), with maximum surface elevation around 1800 m.

The present rate of uplift, measured by geodetic methods, has a maximum value of 1.5–2 mm/a in the Eastern Carpathians, south of the Trotuş Fault (Cornea et al. 1979). Seismologic data provided by M. C. Oncescu from Karlsruhe Geophysical Institute (pers. comm.) indicate the present activity of the Intramoesian and Trotuş sinistral strike-slip faults. A third, dextral strike-slip fault (called here the Sinaia Fault) is constrained south of the Braşov Basin by kinematic data (site 107-95 on Fig. 2, lower corner) and earthquake focal mechanism solutions (Fig. 1a).

The Braşov-Gheorgheni basin system

Starting in Pliocene a series of basins (the Braşov, Ciuc and Gheorgheni basins) were superimposed on Cretaceous-Miocene structures in the internal part of the Eastern Carpathians (see Fig. 1a). We performed a kinematic analysis which indicates a general NW-SE direction of extension, based on methods and data presented in Appendix 1 and Figure 13, and using the computer programs described by Sperner et al. (1993) and Sperner (1996).

The Braşov Basin

The Braşov Basin shows a flat topography around 400 m elevation, surrounded by mountains of up to 1800 m. The basin sedimentary fill is up to 600 m thick and consists of: (A) a fluvial-lacustrine association (Pliocene–Middle Pleistocene), divided into a dominant, clastic facies (with gravel, cross-stratified sand, clay, silt, and lignite deposits), and a subordinate carbonatic-siliceous facies (with limestone, marl, diatomite); (B) an alluvial association (Middle Pleistocene–Holocene) with coarse, migrating channel and alluvial-fan deposits (Marinescu et al. 1981). At different stratigraphic levels the lacustrine sediments are interbedded with andesitic tuffs and lava flows, whose source is in the southern part of the Eastern Carpathian Neogene volcanic chain (Peltz et al. 1971). The faunal assemblages (Liteanu et al. 1962; Samson & Rădulescu 1963; Rădulescu et al. 1965) and magnetostratigraphy (Ghenea et al. 1979) prove an age of 3.6–3.8 Ma for the oldest sediments in the Braşov Basin.

The direction of maximum (σ_1) and minimum (σ_3) calculated paleostresses are considered parallel to the main direction of shortening and extension, respectively. Data collected from Pliocene-Quaternary rocks reveal a NW-SE direction of extension, with strike-slip motion along the NW-SE oriented margins of the basin (Fig. 2; see Table 1 for the results of kinematic analysis). The fault-slip data sets from pre-Pliocene rocks are heterogeneous, indicating different tectonic events. However, the youngest data sub-sets, separated on overprinting criteria of faults of different relative age, show also a NW-SE direction of extension. This direction is therefore assumed to indicate the same deformation event as recorded in the Pliocene-Quaternary rocks, an assumption supported by previous paleostress analyses which report no extension in the southern Eastern Carpathians before Pliocene time (Linzer 1996; Zweigel 1995). The joint data also show a general NW-

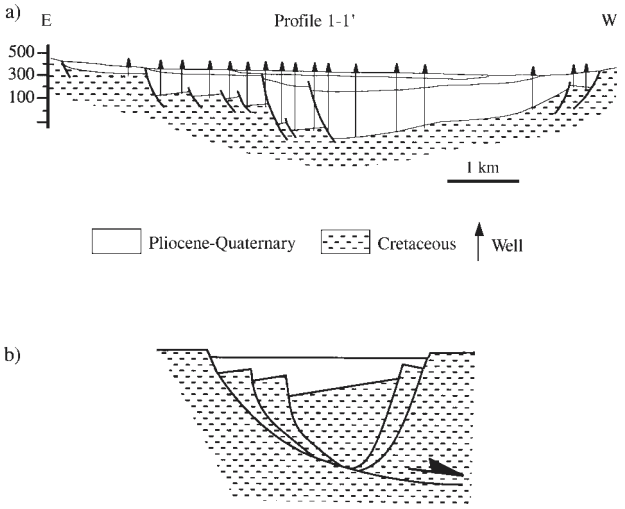

Fig. 3. Profile in the Braşov Basin (see location in Fig. 2) based on well data from Geolex Harghita Exploration Company **(a)**, and used to assume a listric geometry of an asymmetric basin formed above a horizontal detachment fault **(b)**.

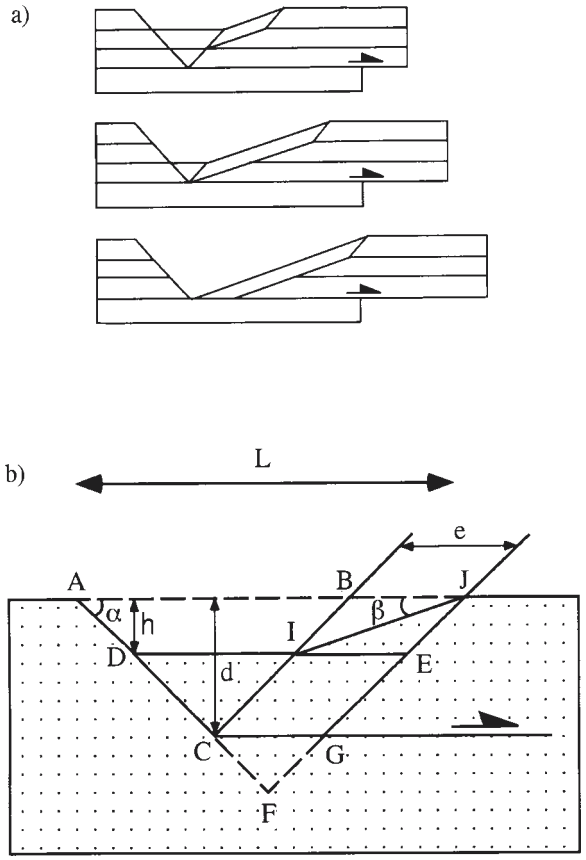

Fig. 4. a) Area-balanced kinematic model for asymmetric basin formation above a horizontal detachment fault (after Groshong 1989). **b)** This model allows calculation of the amount of extension and depth of the detachment fault, based on simple geometric data: a — near-surface plunge of the main detachment fault; b — dip of the antithetic zone; h — basin depth; L — basin width; d — depth of the detachment fault, $d = h(L-e)/e$; e — amount of extension, $e = 2h/\tan\alpha$. For the Braşov Basin d = 8.7 km and e = 14 %.

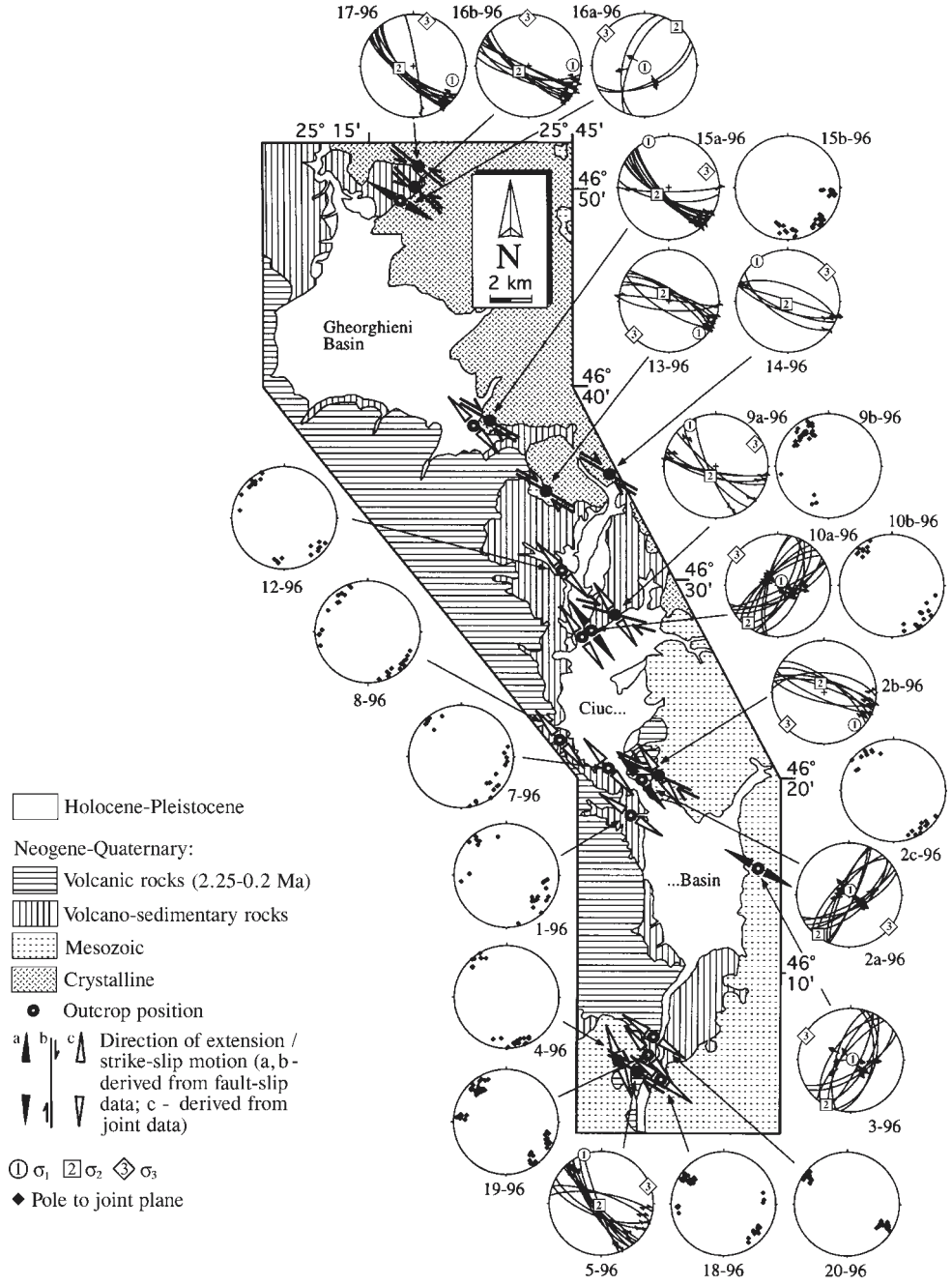

Fig. 5. Geological map of the Ciuc and Gheorghieni Basins (after Alexandrescu et al. 1968; Săndulescu et al. 1968) and directions of extension recorded in Pliocene-Quaternary rocks or separated as the youngest recorded deformation in pre-Pliocene rocks (see Table 1 for results of the kinematic analysis). The fault planes are graphically represented in equal area, lower hemisphere stereonets as great circles, with arrows showing the direction of slip of the hangingwall. The joint planes are plotted in equal area, lower hemisphere stereonets as poles. The calculated stress tensor from fault slip data is defined as the orientation and magnitude of principal stresses $\sigma_1 = \sigma_2 = \sigma_3$, where the main direction of shortening is parallel with σ_1 and the main direction of extension is parallel with σ_3.

SE direction of extension in places, but some joint sets have varying orientation (see Fig. 12) which indicates a stress regime with radial extension. The relative age relationship between these structures suggests that the joint sets with varying orientation are older than the normal faults.

Well data of a Romanian exploration company (Geolex Harghita) were used to infer the geometry of the Braşov Basin. The profile in Figure 3 shows an asymmetric basin shape and tilted blocks, characteristic for listric fault geometry. Therefore, we used a model of asymmetric basin formation along listric faults and above a horizontal detachment fault (Fig. 4a; Groshong 1989) to calculate the amount of extension and the depth of the detachment fault in the Braşov Basin. Figure 4b shows the geometric elements of this model. The basin asymmetry results from the difference between the dip a of the main listric fault on one basin margin and the dip b of the so-called "anti-

thetic zone" on the opposite basin margin. At the first increments of strain the conjugate fault (BC) to the main listric fault (ADCG) is formed, and extension moves the segment BC to a new position JG. The folding of the footwall initiates with BC and JG as axial surfaces. This model is area-balanced when the area of ABC equals the area of DIJEGC. From this condition one obtains the amount of simple shear extension (and total displacement on the horizontal detachment fault) as $e = 2h/\tan\alpha$. The depth of the detachment fault is $d = h(L-e)/e$. For the Braşov Basin a calculation along the line A–A' (shown in Fig. 2) — with L = 16.5 km, h = 1222 m, and a assumed to be 50° (from field observation) — yields a minimum value of extension e = 2 km and depth of the detachment fault d = 8.7 km. A value of 14 % extension is calculated from the "stretched" length L of 16.5 km after 2 km extension. For the whole width of the Braşov Basin the amount of extension is probably not larger than 5 km.

The Ciuc and Gheorgheni basins

Both basins show the same type of sedimentary fill: a fluvial-lacustrine facies with gravel sand, clay and coal, with an important amount of volcano-sedimentary deposits; and an alluvial facies, with river terraces and recent alluvium. The sedimentary pile reaches up to 800 m thickness in the Ciuc Basin and 1000 m in the Gheorghieni Basin, with an age of Pliocene–Early Pleistocene for the fluvial-lacustrine facies and Middle Pleistocene–Recent for the alluvial facies (Bandrabur & Codarcea 1974). K/Ar dating of the youngest lava flow situated below the first sediments deposited in the Ciuc Basin yielded an age of 4.0 ± 0.4 Ma (Pécskay et al. 1995).

Similar to the Braşov Basin, the kinematic analysis indicates NW-SE extension, with strike-slip motion along the NW-SE oriented basin margins (Fig. 5).

The Foreland

North of the Trotuş Fault the subsidence in the Eastern Carpathians foreland occurred only in Sarmatian time. South of this fault the subsidence started in Early Sarmatian (Săndulescu et al. 1981) and continued until Quaternary time. During this period the foreland formations record a change from silty, sandy and gravelly to gravel-dominated sedimentation (Marinescu et al. 1981; Săndulescu et al. 1981). The deposition rate increased from up to 5000 m thickness in Early Sarmatian–Pliocene time (with a mean value of 0.42 mm/a between 13.6–1.9 Ma), to 3000 m in the Pleistocene (1.6 mm/a, after Liteanu et al. 1972). The age and thickness of sediments deposited in the Eastern Carpathians foreland were used by Artyushkov et al. (1996) to infer an uplift curve (Fig. 6) with a very rapid rate during Pliocene–Quaternary time. The young

Table 1: The results of the kinematic analysis of data collected in the Braşov Basin (fault-slip and joint data). Ages: Pz — Paleozoic; J — Jurassic; Cr — Cretaceous; Mc — Miocene; Pl — Pliocene; P — Pleistocene; H — Holocene; E — Early; L — Late. [1] Data sets consisting exclusively of joints are those where only σ_3 is given, as the direction of maximum density of joint poles. [2] R is the ratio between the stress magnitudes [$R = (\sigma_2-\sigma_3)/(\sigma_1-\sigma_3)$]. R defines the regime of deformation, as: — plain strain, with R = 0.5 (deformation occurs only parallel to σ_1 and σ_3, and $\sigma_1 = \sigma_3$, $\sigma_2 = 0$); — axial extension (constriction), with R = 1 (shortening occurs parallel to both σ_1 and σ_2); — axial shortening (flattening), with R = 0 (extension occurs parallel to both σ_2 and σ_3). [3] F indicates the average value of the differences between the measured striae on fault planes and the orientation of the calculated maximum compressive stress (σ_1).

No.	Age	Location Lat. N/Long E	Bed Dip	No. of data	σ_1	σ_2	σ_3 [1]	R [2]	F [3]
1-95	Cr	45°46'38"/25°40'30"	054/12	4	074/11	325/59	170/29	0.546	10°
3-95	EP	45°48'00"/25°40'27"	220/12	61			132/9		
8a-95	EP	45°52'27"/25°36'32"	124/07	11	124/76	247/08	338/02	0.307	16°
8b-95	EP	45°51'03"/25°37'42"	128/10	36			316/2		
10-95	ECr	45°52'24"/25°54'31"	284/37	49			320/20		
11-95	EP	45°57'53"/25°50'46"		3	347/76	252/1	162/14	0.499	1°
12-95	ECr	45°57'39"/24°48'56"	125/46	46			320/8		
13-95	EP	45°55'00"/25°47'28"		29			313/2		
14a-95	EP	45°52'30"/25°46'38"	119/05	8	100/86	234/3	324/3	0.434	12°
14b-95	EP	45°52'30"/25°46'38"	119/05	32			302/10		
15-95	EP	45°46'23"/25°45'18"		23			307/5		
16-95	ECr	45°55'22"/25°59'00"	021/16	35			127/3		
17-95	EP	45°55'49"/26°00'08"		52			307/27		
18a-95	Cr	45°58'46"/26°00'52"	274/70	9	307/84	59/2	150/5	0.444	10°
18b-95	Cr	45°58'46"/26°00'52"	274/70	22			140/5		
19-95	ECr	46°00'04"/26°01'10"	199/24	33			139/6		
20-95	ECr	46°01'52"/26°02'02"	215/61	24			137/3		
21-95	EP	46°03'01"/26°02'09"		3	163/15	3/74	254/5	0.501	2°
22-95	ECr	46°03'01"/26°01'48"	234/55	28			315/2		
23a-95	Ec	46°03'01"/26°07'54"	291/24	4	144/77	48/2	317/18	0.504	2°
23b-95	Ec	46°02'56"/26°07'54"	291/24	28			308/9		
24-95	Ec	46°04'59"/26°09'55"	283/19	18			136/2		
26-95	ECr	45°53'32"/25°36'02"	293/60	23			321/3		
28-95	EP	46°04'42"/25°36'49"	102/15	25			308/7		
29-95	EP	46°06'50"/25°34'31"	128/16	16	226/89	41/1	131/0	0.401	12°
103-95	ECr	45°54'18"/25°28'32"	140/65	9	308/89	47/0	137/1	0.474	8°
103o-95	ECr	45°54'18"/25°28'32"	140/65	10	129/22	284/63	34/10	0.866	13°
104-95	ECr	45°51'22"/25°29'00"	230/17	12	150/86	47/1	317/4	0.510	18°
104o-95	ECr	45°51'22"/25°29'00"	230/17	12	295/2	29/86	295/4	0.525	5°
105-95	ECr	45°50'02"/25°27'08"	135/19	11	253/85	51/5	141/2	0.431	15°
105o-95	ECr	45°50'02"/25°27'08"	135/19	8	300/6	44/67	208/20	0.261	13°
107a-95	Ec	45°33'21"/25°18'10"	160/47	12	206/65	19/48	113/3	0.591	8°
107b-95	Ec	45°33'21"/25°18'10"	160/47	9	156/14	31/66	251/19	0.556	9°
110-95	J	45°37'40"/25°29'58"		9	127/79	238/4	329/11	0.377	10°
115a-95	J	45°38'31"/25°37'00"		13	19/78	243/98	151/8	0.336	21°
115b-95	J	45°38'31"/25°37'00"		23	105/28	313/59	202/12	0.358	21°

Continuation of Table 1

No.	Age	Location Lat. N/Long E	Bed Dip	No. of data	σ_1	σ_2	σ_3[1]	R^2	F[3]
1-96	Pl	46° 18' 02" /25° 47' 24"		22			123/24		
2a-96	Pl	46° 19' 41" /25° 49' 16"		11	20/84	218/5	128/2	0.486	10°
2b-96	Pl	46° 19' 41" /25° 49' 16"		8	138/14	337/75	229/5	0.485	7°
2c-96	Pl	46° 19' 41" /25° 49' 16"		19			144/7		
3-96	Cr	46° 15' 53" /25° 58' 39"	144/43	10	106/87	208/1	298/3	0.443	14°
4-96	Cr	46° 05' 42" /25° 04' 22"	111/16	20			158/8		
5-96	Pl	46° 04' 58" /25° 50' 04"		12	340/1	232/86	70/4	0.556	10°
7-96	LMc-Pl	46° 20' 18" /25° 48' 10"		21			138/3		
8-96	LMc-Pl	46° 21' 52" /25° 42' 02"		22			139/4		
9a-96	LMc-Pl	46° 27' 53" /25° 46' 57"		7	327/8	210/74	59/14	0.534	14°
9b-96	LMc-Pl	46° 27' 53" /25° 46' 57"		28			325/24		
10a-96	LMc-Pl	46° 27' 39" /25° 42' 21"		14	46/83	217/7	307/1	0.453	12°
10b-96	LMc-Pl	46° 27' 39" /25° 42' 21"		29			322/3		
12-96	LMc-Pl	46° 30' 45" /25° 44' 52"		21			136/4		
13-96	Pz	46° 36' 02" /25° 48' 04"		5	323/3	203/84	53/5	0.455	13°
14-96	Pz	47° 37' 30" /25° 44' 14"		8	136/13	331/76	227/3	0.481	9°
15a-96	Pz	47° 37' 53" /25° 37' 27"		12	336/3	239/69	67/21	0.534	7°
15b-96	Pz	47° 37' 53" /25° 37' 27"		35			137/12		
16a-96	Pz	46° 50' 22" /25° 29' 03"		4	163/87	40/2	310/3	0.362	16°
16b-96	Pz	46° 50' 22" /25° 29' 03"		9	90/15	242/73	358/8	0.493	5°
17-96	LMc-	46° 51' 22" /25° 25' 54"		9	111/20	262/67	17/10	0.474	3°
18-96	P-H	46° 04' 44" /25° 50' 33"		36			306/17		
19-96	Pl	46° 06' 30" /25° 50' 44"		47			319/20		
20-96	Pl	46° 07' 22" /25° 51' 13"		29			304/4		
22-96	Pl-P	46° 01' 51" /25° 25' 52"		25	245/86	48/4	138/1	0.452	12°
23-96	Pl-P	46° 01' 45" /25° 24' 32"		11	215/86	59/4	329/2	0.524	6°
24-96	Pl-P	46° 01' 14" /25° 24' 31"		6	359/85	220/4	130/3	0.456	10°
25-95	Pl-P	45° 57' 22" /25° 21' 17"		17	23/87	221/3	131/1	0.476	10°
26-96	Pl-P	45° 59' 26" /25° 19' 35"		12	123/85	232/2	322/4	0.478	6°
27-96	Pl-P	45° 53' 30" /25° 53' 10"		18	9/88	226/2	136/1	0.427	11°
34-96	Cr	45° 42' 02" /25° 18' 14"		11	188/40	347/48	88/11	0.623	21°

uplift of the southern Eastern Carpathians is indicated also by fission-track data which yielded 2 Ma for the youngest cooling ages (Sanders et al. 1997).

The foreland area situated between the Trotuş and the Intramoesian faults was folded in Pliocene–Pleistocene time, during the "Valachian Phase" (Săndulescu 1984). The absence of good exposure in this area makes a paleostress analysis, based on fault-slip data, impossible; but published geological maps (Motaş et al. 1967; Dumitrescu et al. 1968a; Dumitrescu et al. 1968b) show NNE-SSW (in the N) to ENE-WSW (in the S) trending regional fold axes (Fig. 1a) which indicate a general NW-SE oriented shortening.

The Perşani volcanics

Alkali basaltic volcanism was active in the Perşani Mts., NW of the Braşov Basin (Fig. 1a), during Pliocene–Quaternary time. K/Ar analyses yielded ages of 2.25–0.35 Ma for the volcanic activity (Casta 1980; Mihăilă & Kreutzer 1981; Downes et al. 1995). The kinematic analysis of fault-slip data collected from the Perşani basalts shows a general NW-SE direction of extension (Fig. 7), expressed in outcrop-scale normal faults, domino and horst-and-graben structures (Fig. 8). The ubiquitous distribution of these extensional structures within the volcanic chain and their constant orientation excludes, in our opinion, the possibility that they were formed due to "non-tectonic" processes, for instance caldera collapse or updoming due to shallow intrusions (as argued by Seghedi & Szakács 1994). The calculated direction of extension and the NE-SW oriented alignment of the eruption centres indicate the emplacement of the basalts along a NE-SW-trending crustal fracture.

The kinematic model

Our kinematic data prove that the extension initiated in the Braşov Basin through jointing, because the joints are older than the normal faults. According to general accepted genetical interpretations for joints

Table 2: Seismological data of earthquakes occurred along the Trotuş, Sinaia, and Intramoesian strike-slip faults. The data were provided by M.C. Oncescu (Karlsruhe University), and calculated after the P wave first motion signs. Each focal mechanism solution is accompanied by an information set, consisting of: — earthquake number, used to identify the plot on the map in Figure 1a; — date when the earthquake occurred, (year, month, day); — epicenter co-ordinates (in decimal values); — focal depth; — magnitude (MB — body wave magnitude; MS — surface wave magnitude; ML — local magnitude, based on duration of seismic oscillations); — focal plane data: strike (s), dip (d), and rake (r) of the nodal planes, and orientation of the P, B, and T axes (a — azimuth, p — plunge). The P and T axes are assumed parallel to the directions of the maximum shortening and extension, respectively.

No.	Date Year, Mo, Dy	Lat. N	Long. E	Depth	Magnitude MB, MS, ML	Nodal plane A s, d, r	Nodal plane B s, d, r	P axis a, p	B axis a, p	T axis a, p
35	1960, 01, 04	46.260	26.770	41	5.4 MS	220, 90	130, 65	88, 18	220, 65	352, 18
44	1967, 02, 27	44.860	26.690	32	5.0 MB	187, 71	289, 61	145, 36	337, 53	239, 8
46	1969, 04, 18	45.300	25.100	10	5.2 ML	137, 83	231, 60	90, 26	304, 60	187, 16
48	1975, 02, 08	45.100	26.000	23	4.7 ML	144, 74	48, 70	7, 27	179, 63	274, 3
49	1975, 03, 07	44.900	26.600	21	5.1 ML	237, 83	143, 60	6, 15	247, 60	104, 26

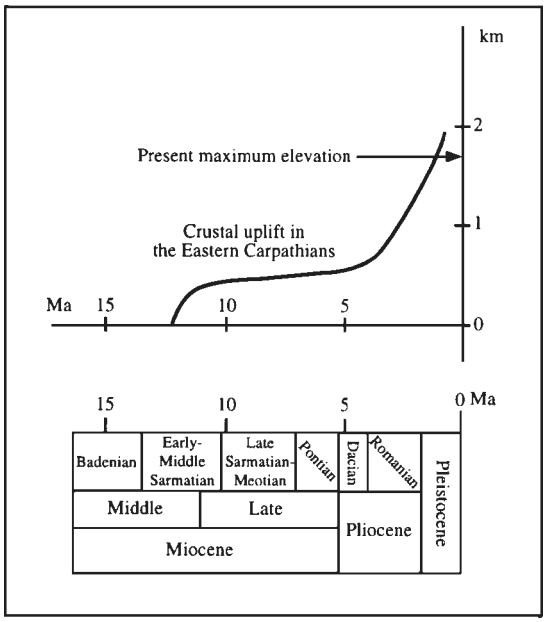

(see Ramsay & Huber 1987, and references therein), we suggest that regional uplift was the driving mechanism for the formation of the vertical extensional fractures in the Braşov Basin. The potential energy stored in rocks in a region subjected to uplift increases with increasing elevation and, later, a deviatoric horizontal stress will result from the potential energy contrast between the uplifted area and the surroundings (Houseman & England 1986). When the uplift-induced horizontal deviatoric stress is large enough to exceed rock strength, extension begins in terms of "gravity spreading" (Neugebauer 1978), due to gravitational mass transfer from the area with higher potential energy towards the area with lower potential energy. For the Braşov Basin we suggest that the magnitude of extensional strain was ini-

Fig. 6. Uplift curve in the Eastern Carpathians (after Artyushkov et al. 1996). The presence of 3000 m thick Pleistocene formations in the Eastern Carpathians foreland basin (Liteanu et al. 1972) suggests a higher pre-Quaternary elevation of the Eastern Carpathians than the present elevation.

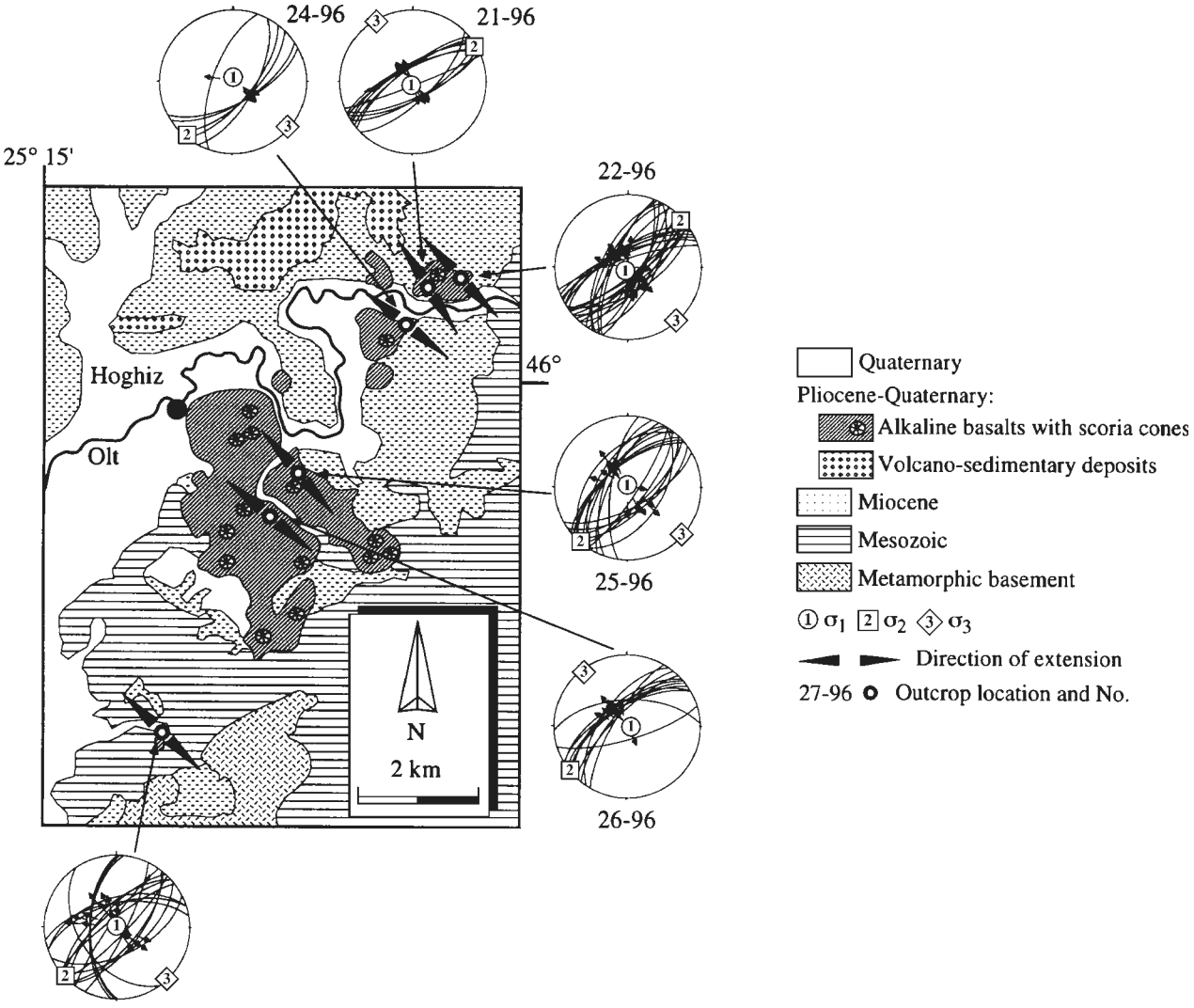

Fig. 7. Geological map of the Perşani Mts. (after Patrulius et al. 1967; Săndulescu et al. 1968; Seghedi & Szakács 1994) and directions of extension recorded in Pliocene-Quaternary alkaline basalts. For further explanation, see Figure 5.

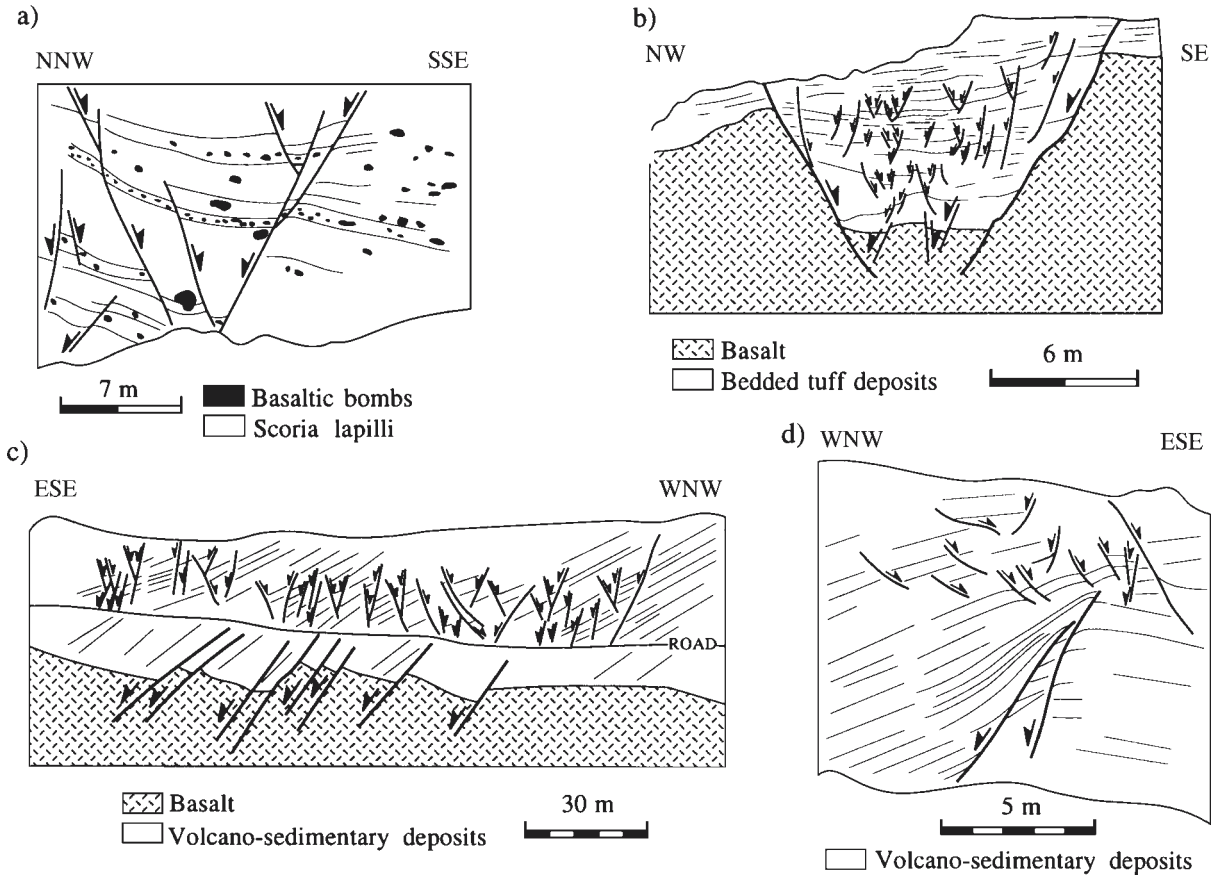

Fig. 8. Tectonic structures from the Perşani Mts. indicating NW-SE oriented extension in the Pliocene-Quaternary basaltic/volcano-sedimentary rocks (in quarries): **a)** Hegheş (outcrop 21-96); **b)** Mateiaş (outcrop 24-96); **c, d)** La Brazi (outcrop 22-96).

tially small and the extension had rather a radial orientation, since joints with varying orientation formed; in a later stage the normal faults developed, accomodating increasing extensional strain due to an increasing topographic gradient. The dominance of NW-SE oriented extension may be directly related to the presence of available space in the corner between the European and the Moesian plates (see Fig. 1a). This available space is considered a free boundary which allowed mass transfer from the uplifted area. Thus, the uplift-related extension from the hinterland was accommodated by shortening in the foreland.

A kinematic model is presented here (Fig. 9) taking into account the observed strike-slip faults on the basin borders. In our model the gravitational, uplift-induced southeastward motion of a crustal block between the sinistral Trotuş and the dextral Sinaia strike-slip faults resulted in extension in the hinterland accommodated by shortening in the foreland. The calculated amount of extension in the Braşov Basin is e = 14 % (probably not larger than 5 km), above a detachment fault at ca. 8.7 km minimum depth (our calculation). This detachment may have been connected with older detachment horizons at 10–15 km depth, shown by Ştefănescu (1985) in the Eastern Carpathians flysch nappes (Fig. 10). These detachment horizons were reactivated in Pliocene time and transferred the deformation from the hinterland to the foreland. The present subsidence in the Braşov Basin (up to 4 mm/a after Cornea et al. 1979) and seismicity along the Trotuş and Sinaia faults, together with the shallow earthquakes indicating NW-SE horizontal compression within the fold-and-thrust belt, fit in this model and can be explained by it.

The NW-SE to N-S oriented Pliocene-Quaternary shortening from the outer southern Eastern Carpathians has been related to a southward displacement of the orogen relative to its foreland (Hippolyte & Săndulescu 1996). However this shortening may have partly accomodated the extension from the Braşov-Gheorghieni basins, as we propose in our model.

Conclusion

Rapid uplift in the Eastern Carpathians starting in Pliocene time resulted in gravity-induced southeastward motion of a crustal block above reactivated detachment horizons from the fold-and-thrust belt, in an area between the Trotuş and the Sinaia strike-slip faults. The motion of this crustal block resulted in NW-SE oriented extension and the formation of the Braşov-Gheorghieni basins in the hinterland, accommodated by shortening and folding of the foreland formations in the foreland, in the available space inside the corner between the European and Moesian plates. The amount of Pliocene-Quaternary hinterland extension (and, consequently, of foreland shortening) is around 5 km. The zone of folded Pliocene-Quaternary foreland formations between the Sinaia and the Intramoesian faults (see Fig. 1a) still can not be ex-

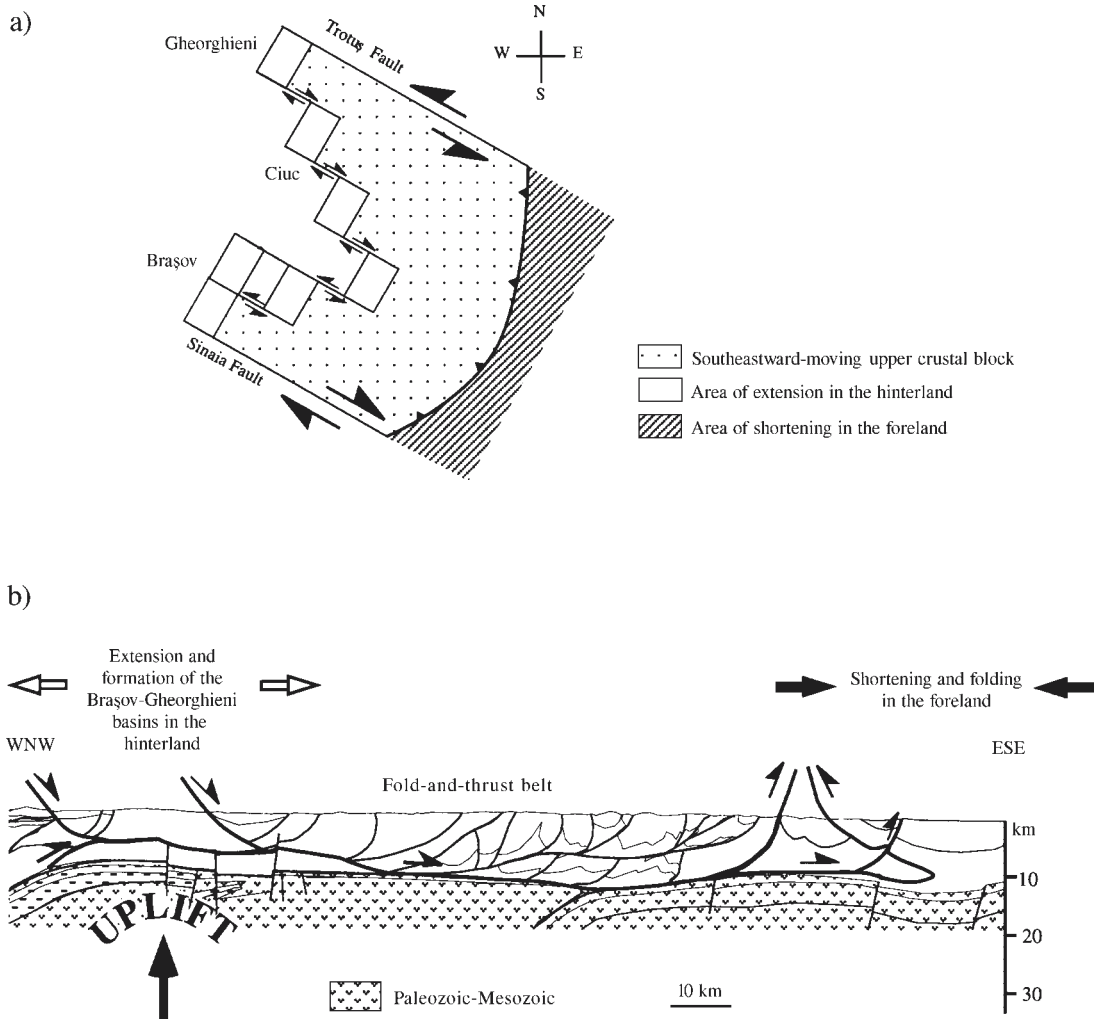

Fig. 9. a) Kinematic model for the Pliocene to Recent tectonic evolution of the Eastern Carpathians. The uplift-induced southeastward motion of a crustal block between the Trotuş and Sinaia strike-slip faults resulted in extension and basin formation in the hinterland, accommodated by coeval shortening and folding in the foreland; **b)** the crustal motion may have been taken place above a detachment horizon within the fold-and-thrust belt (profile after Ştefănescu 1985).

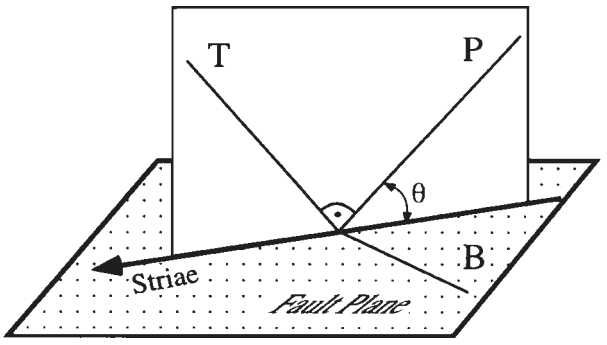

Fig. 10. Geometric assumptions used for kinematic analysis. For a given fault plane and striae (with known sense of slip), the shortening axis P (parallel to σ_1) and the extension axis T (parallel to σ_3) lie in a plane normal to the fault plane, containing the slip line (after Turner 1953). The B axis (parallel to σ_2) is normal both to P and T axes. The angle θ is a function of the slope of the Mohr envelope.

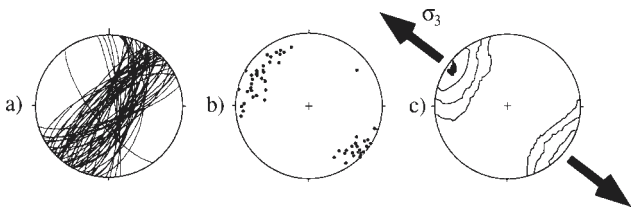

Fig. 11. Example of kinematic interpretation of joint data (outcrop 3-95): **a)** graphical presentation of joint planes in equal area, lower hemisphere stereonets; **b)** poles of the joint planes; **c)** contoured density intervals using the Kamb method of contouring (Kamb 1959). Maximum density (the black area) is assumed to be parallel to the main direction of extension (σ_3).

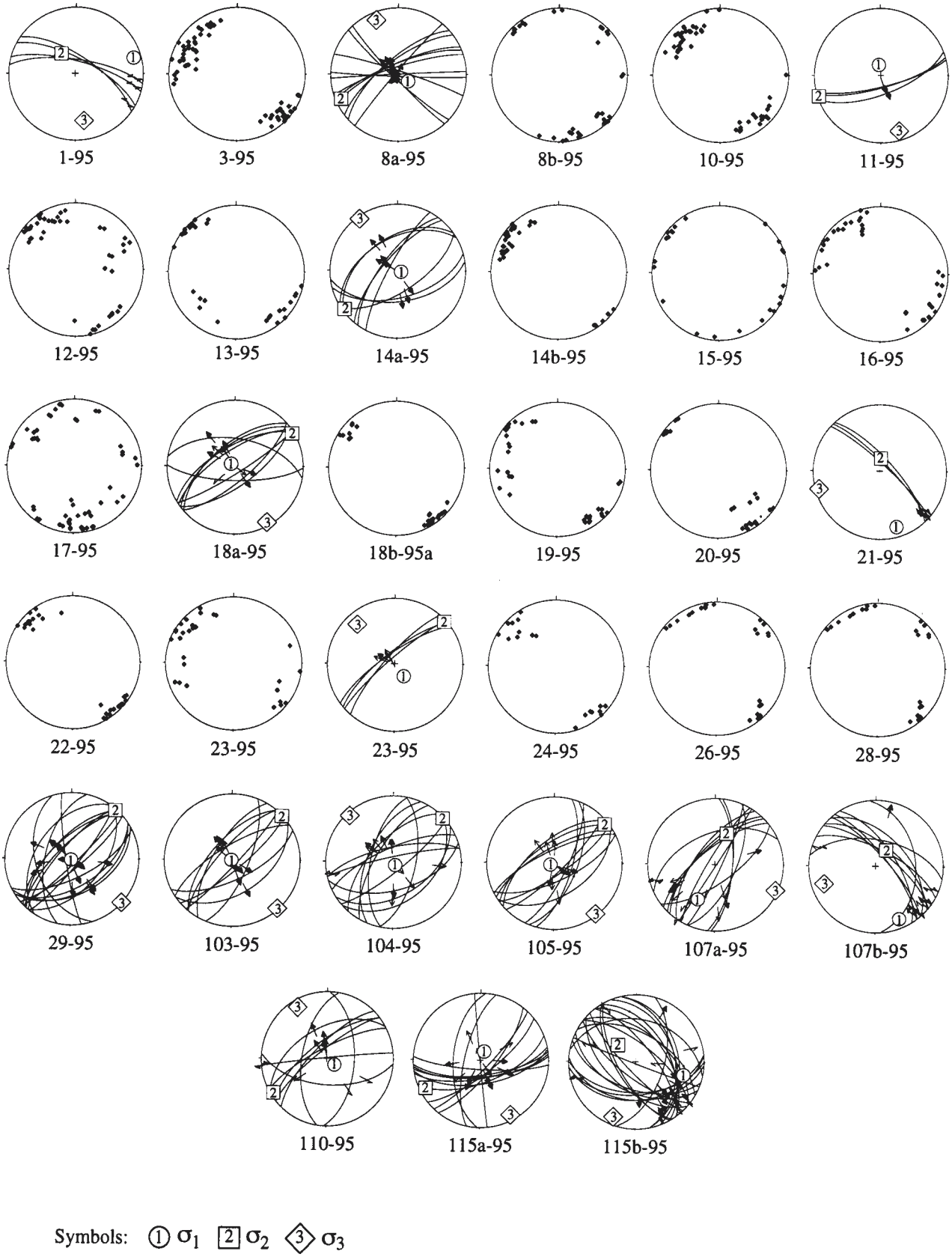

Fig. 12. Graphical presentation of fault-slip and joint data collected in the Braşov Basin. The fault planes are represented in equal area, lower hemisphere stereonets as great circles, with arrows showing the direction of slip on the hangingwall. The joint planes are plotted in equal area, lower hemisphere stereonets as poles. See data locations in Fig. 2.

plained with this model. The shortening there may be related to the general N-S compression recorded in the Moesian Platform by Bergerat et al. (1995) and Maţenco (1997). Another open question remains the mechanism which induced the accelerated rate of uplift in Pliocene time, 5–6 Ma after the Miocene oceanic closure. A model presented by Gîrbacea & Frisch (1998) suggests delamination of the lower lithospheric mantle, following continental collision and slab break-off, as the uplift-triggering mechanism.

Acknowledgments: Financial support was given by the German Science Foundation. We had stimulating discussions with Horst-Peter Hann, Lothar Ratschbacher, Franz Moser, Blanka Sperner, and Peter Zweigel. Helpful reviews were given by Franz Neubauer and Michal Kováč. All this is gratefully acknowledged.

Appendix

The methods and results of kinematic analysis

The orientation of faults and associated striae can be used to determine the stress tensor, defined as the orientation of principal stresses $\sigma_1 = \sigma_2 = \sigma_3$ and the ratio R between the stress magnitudes $[R = (\sigma_2 - \sigma_3)/(\sigma_1 - \sigma_3)]$, during a brittle episode of deformation. Although the kinematic analysis calculates the main directions on which "strain" (deformation) occurred, the term "stress" is used here (paleostress analysis, stress tensor, stress ratio, etc.) because it is used in most of the publications, in fact dealing with strain analysis. The geometric assumption used for the kinematic analysis of fault-slip data is presented in Figure 11. For a given fault plane and associated striae (defined by their direction and sense of slip), the σ_1 axis lies in the plane defined by the slip direction and the normal to the fault plane. The angle θ between the σ_1 and the slip direction (which is, in fact, the angle between the developing fault and the principal axis of the compression) is a function of the slope of the Mohr envelope and has a maximum value of 45^o due to the Coulomb failure criterion. The fault planes are graphically represented in equal area, lower hemisphere stereonets as great circles, with arrows showing the direction of slip of the hangingwall. The aim of the kinematic analysis is to calculate the best fitting stress tensor for a fault population, applying these geometrical conditions to each fault (see Allmendinger et al. 1989, and references therein for further discussions on this topic).

For the kinematic analysis of joint data the joint planes were plotted in equal area, lower hemisphere stereonets as poles (see Figs. 5 and 12). The maximum density of poles to joint planes was assumed to indicate the direction of maximum extension, i.e. σ_3. A contouring procedure was applied to each data set to derive the maximum density of joint poles, following the method of Kamb (1959). This method calculates the magnitude of standard deviation " σ" (not to relate to stress terminology) for a uniform distribution of points on the projection. The resulting plot shows fields of point density, the maximum density being assumed to indicate the direction of maximum extension (Fig. 12). The data sets with joints with varying orientation were assumed to indicate a stress regime with radial extension and flattening geometry (i.e. with extension occurring parallel to both σ_2 and σ_3).

References

Alexandrescu Gr., Mureşan G., Peltz S. & Săndulescu M., 1968: Geological Map of Romania, Scale 1:200,000, Odorhei Sheet. *Geological Institute,* Bucharest.

Allemendinger R.D., Gephard L.W. & Marrett R.A., 1989: Notes on fault slip analysis. *Geological Society of America, Short Course,* 1–68.

Artyushkov E.V., Baer M.A. & Mörner N.-A., 1996: The East Carpathians: indications of phase transitions, lithospheric failure and decoupled evolution of thrust belt and its foreland. *Tectonophysics,* 262, 101–132.

Bandrabur T., Ghenea C., Săndulescu M. & Ştefănescu M., 1971: Neotectonic Map of Romania, Scale 1:1,000,000. *Geological Institute,* Bucharest.

Bandrabur T. & Codarcea V., 1974: Contribuţii la cunoaşterea depozitelor plio-cuaternare din regiunea cursului superior al Mureşului. *Studii Tehnice şi Economice,* Bucharest, H, 5, 23–60.

Bergerat F., Martin P. & Dimov D., 1995: The Moesian Platform as a piece of the Carpatho-Balkan puzzle in the framework of the Tethys evolution. *Terra Nova,* 7, *Abstract Suppl.* 1, 181.

Casta I., 1980: Les formation Quaternaires de la depression de Braşov. *Thèse Univ. D'Aix Marseille,* 1–256.

Cornea I., Drăgoescu I., Popescu M. & Visarion M., 1979: Harta mişcărilor crustale verticale recente pe teritoriul R.S. România. *Studii şi Cercetări de Geologie, Geofizică, Geografie, Seria Geofizică,* Bucharest, 17, 1, 3–17.

Csontos L., 1995: Tertiary tectonic evolution of the Intra-Carpathian area. *Acta Vulcanologica*, 7, 2, 1–13.

Csontos L., Nagymarosy A., Horváth F. & Kováč M., 1992: Tertiary evolution of the intra-Carpathian area; a model. *Tectonophysics,* 208, 1–3, 221–241.

Downes H., Seghedi I., Szakács A., Dobosi G., James D.E., Vaselli O., Rigby I.J., Ingram G.A., Rex D. & Pécskay Z., 1995: Petrology and geochemistry of late Tertiary/ Quaternary mafic alkaline volcanism in Romania. *Lithos,* 35, 1–2, 65–81.

Dumitrescu I. & Săndulescu M., 1968: Problémes structuraux fondamentaux des Carpathes roumaines et de leur Avant-pays. Anuarul Comitetului Geologic, XXXVI. *Geological Institute,* Bucharest, 195–218,

Dumitrescu I., Săndulescu M., Bandrabur T. & Săndulescu J., 1968a: Geological Map of Romania, Scale 1:200,000, Covasna Sheet. *Geological Institute,* Bucharest.

Dumitrescu I., Mirăuţă O., Săndulescu M., Ştefănescu T. & Bandrabur T., 1968b: Geological Map of Romania, Scale 1:200,000, Bacău Sheet. *Geological Institute,* Bucharest.

Fuchs K., Bonjer K., Bock G., Cornea I., Radu C., Enescu D., Jianu D., Nourescu A., Merkler G., Moldoveanu T. & Tudorache G., 1979: The Romanian earthquake of March 4, 1977; II, Aftershocks and migration of seismic activity. *Tectonophysics,* 53, 3–4, 225–247.

Ghenea C., Andreescu I., Bandrabur T., Cepalîga A., Mihăilă N. & Trubihin V., 1979: Bio- and magnetostratigraphic correlations on the Pliocene and Lower Pleistocene Formations of the Dacic Basin and Braşov Depression (East Carpathians). *Dări de Seamă ale Institutului de Geologie şi Geofizică (Bucharest),* LXVI, 139–156.

Gîrbacea R. & Frisch W., 1998: Slab in the wrong place: Lower lithospheric mantle delamination in the last stage of the Eastern Carpathian subduction retreat. *Geology,* 26, 7, 611–614.

Groshong R.H., Jr., 1989: Half-graben structures; balanced models of extensional fault-bend folds. *Geol. Soc. Amer. Bull.,* 101, 1, 96–105.

Houseman G. & England Ph., 1986: A dynamical model of lithosphere extension and sedimentary basin formation. *J. Geophys. Res.,* 91, B1, 719–729.

Kamb W.B., 1959: Theory of preferred crystal orientation developed by crystallization under stress. *J. Geol.,* 67, 2, 153–170.

Linzer H.-G., 1996: Kinematics of retreating subduction along the Carpathian Arc, Romania. *Geology*, 24, 2, 167–170.

Liteanu E., Mihăilă N. & Bandrabur T., 1962: Contribuţii la studiul stratigrafiei Cuaternarului din bazinul mijlociu al Oltului. *Studii şi Cercetări de Geologie, (Bucharest),* 1, VII, 485–511.

Liteanu E., Feru M. & Ghenea A., 1972: Cuaternarul din zona de curbură a Carpaţilor Orientali dintre văile Cîlnău şi Milcov. *Studii Tehnice şi Economice, Geological Institute,* Bucharest, H, 4, 7–27.

Marinescu F., Ghenea C. & Papaianopol I., 1981: Stratigraphy of the Neogene and the Pleistocene Boundary. *Guide to Excursion A6, Carpatho-Balkan Geological Association, Geological Institute,* Bucharest, 111.

Maţenco L.C., 1997: Tectonic evolution of the outer Romanian Carpathians. *PhD thesis, Vrije University*, Amsterdam, 1–160.

Mihăilă N. & Kreutzer H., 1981: Contribuţii la cunoaşterea cronologiei vulcanitelor bazaltice din Perşanii centrali şi sudici. *Terra,* 4, 37–43.

Motaş I., Bandrabur T., Ghenea C. & Săndulescu M., 1967: Geological Map of Romania, Scale 1:200,000, Ploieşti Sheet. *Geological Institute,* Bucharest.

Neugebauer H.J., 1978: Crustal doming and the mechanism of rifting. Part 1, Rift formation. *Tectonophysics,* 45, 159–186.

Oncescu M.C., 1984: Deep structure of the Vrancea region, Romania, inferred from simultaneous inversion for hypocenters and 3-D velocity structure. *Annales Geophysicae,* 2, 1, 23–27.

Paraschiv D., 1979: Romanian oil and gas fields. *Tech. Econ. St.,* Ser. A, 13, 382.

Patrulius D., Gherasi N., Săndulescu M., Popescu I., Popa E. & Bandrabur T., 1967: Geological Map of Romania, Scale 1:200,000, Braşov Sheet. *Geological Institute,* Bucharest.

Pécskay Z., Edelstein O., Seghedi I., Szakács A., Kovacs M., Crihan M. & Bernad M., 1995: K-Ar datings of Neogene-Quaternary calc-alkaline volcanic rocks in Romania. *Acta Vulcanologica,* 7, 2, 53–62.

Peltz S., Vasiliu C. & Bratosin I., 1971: Petrologia rocilor bazaltice Plio-Cuaternare din România. *Anuarul Institutului de Geologie şi Geofizică, Bucharest,* XXXIX, 111–175.

Ramsay J.G. & Huber M.I., 1987: The techniques of modern structural geology. Volume 2: Folds and fractures. *Academic Press Limited,* London, 1–393.

Rădulescu C., Kovacs Al., Mihăilă N. & Samson, 1965: Contributions à la connaissance des faunes de mammifères pléistocènes de la Dépression de Braşov (Roumanie). *Eiszeitalter und Gegenwart, Öhringen*, 16, 132–188,

Rădulescu D., Cornea I., Săndulescu M., Constantinescu P., Rădulescu F. & Pompilian Al., 1976: Structure de la croúte terrestre en Roumanie—essai d'interprétation des études seismiques profonds. *Anuarul Institutului de Geologie şi Geofizică, Bucharest,* L, 5–36.

Roure F., Roca E. & Sassi W., 1993: The Neogene evolution of the outer Carpathian flysch units (Poland, Ukraine and Romania): kinematics of a foreland/fold-and-thrust belt system. *Sed. Geol.,* 86, 1–2, 177–201.

Royden L.H., 1993: Evolution of retreating subduction boundaries formed during continental collision. *Tectonics,* 12, 3, 629–638.

Samson P. & Rădulescu C., 1963: Les faunes mammalogiques du Pléistocéne inférieur et moyen de Roumanie. *Compte Rendus Hebdomadaires des Seances de l'Academie des Sciences,* 257, 5, 1122–1124.

Sanders C.A.E. & Andriessen A.M., 1996: The relation between tectonics and morphology in a thrust belt: a fission track study from the Eastern Carpathians in Romania. *International workshop on fission-track dating, Gent, Belgium. Abstract Volume,* 96.

Sanders C., Huismans R. & Bertotti G., 1997: The East Carpathians: Deformation in a double vergent orogenic wedge: European Union of Geosciences EUG-9 Conference. *Terra Nova* 9, Abstract Suppl. No. 1, 154.

Săndulescu M., 1984: Geotectonica României. *Editura Tehnică,* Bucharest, 1–336.

Săndulescu M., Vasilescu A.l., Popescu A., Mureşan M., Arghir-Drăgulescu A. & Bandrabur T., 1968: Geological Map of Romania, Scale 1:200,000, Topliţa Sheet. *Geological Institute,* Bucharest.

Săndulescu M., Kräutner H., Borcoş M., Năstăseanu S., Patrulius D., Ştefănescu M., Ghenea C., Lupu M., Savu H., Bercia I. & Marinescu, F., 1978: Geological Map of Romania, Scale 1:1,000,000. *Geological Institute,* Bucharest.

Săndulescu M., Ştefănescu M., Butac A., Pătruţ I. & Zaharescu, 1981: Genetical and structural relations between flysch and molasse (the East Carpathians model). *Guide to Excursion A5, Carpatho-Balkan Geological Association, Geological Institute,* Bucharest, 1–95.

Săndulescu M., Mărunţeanu M. & Popescu Ghe., 1995: Lower-Middle Miocene formations in the folded area of the East Carpathians. *Romanian Journal of Stratigraphy,* 76, 5, 1–32.

Seghedi I. & Szakács A., 1994: Upper Pliocene to Quaternary Basaltic volcanism in the Perşani Mountains. *Romanian Journal of Petrology,* 76, 101–108.

Sperner B., Ratschbacher L. & Ott R., 1993: Fault-striae analysis; a Turbo Pascal program package for graphical presentation and reduced stress tensor calculation. *Computers & Geosciences*, 19, 9, 1361–1388.

Sperner B., 1996: Computer programs for the kinematic analysis of brittle deformation structures and the Tertiary tectonic evolution of the Western Carpathians (Slovakia). *Tübinger Geowissenschaftliche Arbeiten (TGA),* A, 27, 1–120.

Starostenko V.I. & Kharitonov O.M., 1996: East Carpathian-Pannonian connection according to geophysical data. *Mitteilungen der Gesellscahft der Geologie-und Bergbaustudenten in Österreich,* 41, 134–135.

Ştefănescu M., 1985: Geologic Profile, Scale 1:200,000, A-14. *Geological Institute,* Bucharest.

Turner F.J., 1953: Nature and dynamic interpretation of deformation lamellae in calcite of three marbles. *Amer. J. Sci.*, 251, 4, 276–298.

Wagner-Zweigel P., 1995: Structure and kinematics of a bent fold-and-thrust belt; the oil-bearing outer Eastern Carpathians (Romania). *AAPG Bull.*, 79, 8, 1255.